

Towards Closing the Gap in Weakly Supervised Semantic Segmentation with DCNNs: Combining Local and Global Models

Christoph Mayer
ETH Zürich, Switzerland
chmayer@vision.ee.ethz.ch

Radu Timofte
ETH Zürich, Switzerland
timofer@vision.ee.ethz.ch

Grégory Paul
ETH Zürich, Switzerland
grpaul@vision.ee.ethz.ch

Abstract

Generating training sets for deep convolutional neural networks is a bottleneck for modern real-world applications. This is a demanding task for applications where annotating training data is costly, such as in semantic segmentation. In the literature, there is still a gap between the performance achieved by a network trained on full and on weak annotations. In this paper, we establish a strategy to measure this gap and to identify the ingredients necessary to close it.

On scribbles, we establish state-of-the-art results comparable to the latest published ones [29]: we obtain a gap in mIoU of 2.4% without CRF (2.8% in [29]), and 2.9% with CRF post-processing (2.3% in [29]). However, we use completely different ideas: combining local and global annotator models and regularising their prediction to train DeepLabV2.

Finally, closing the gap was reported only recently for bounding boxes [12], by requiring 10× more training images. By simulating varying amounts of pixel-level annotations respecting scribble human annotations statistics, we show that our training strategy reacts to small increases in the amount of annotations and requires only 2–5× more annotated pixels, closing the gap with only 3.1% of all pixels annotated. This work contributes new ideas towards closing the gap in real-world applications.

1. Introduction

Semantic segmentation aims at extracting *semantically meaningful* segments and classify each part into one of the classes predefined by the user. It is a central problem to computer vision, because it bridges a lower-level task (image segmentation) to a higher-level one (scene understanding). State-of-the-art models are data-driven and require for training examples of images together with the segmentation of the intended classes. Recently, Deep Convolutional Neural Networks (DCNNs) have achieved the best performance

to date on the public data sets used for comparing different frameworks in a normalized fashion [7], such as PASCAL VOC [6] or MS-COCO [17].

However, DCNNs are typically greedy in the amount of training data. For semantic segmentation, providing a training set is a demanding task, because it requires assigning carefully a label to each pixel in the training set. This poses two problems for real-world applications of semantic segmentation: *versatility* and *scalability*. Versatility is an issue when the classes of interest differ from the ones in the training set: this requires re-annotating the training images. Scalability is an issue when the number of training images grows significantly, *i.e.* at the scale of data sets that are nowadays available and required in real-world applications.

1.1. Weakly-supervised Semantic Segmentation

A solution to these issues is to rely on *weak supervision*. In semantic segmentation, a *full annotation* holds information about the location, the shape, the spatial relationships between segments, the co-occurrence of classes, the class of each segment, etc. In contrast, *weak annotations* do not provide direct examples of semantic segments, but offer only partial cues: image-level tags provide class information [22, 11], point supervision provides class and approximate location [1], bounding boxes [12] provide class, approximate location and extent, scribbles [16, 31, 29] provide class, approximate object location and potentially extent and can annotate stuff. On one hand, weak annotations are easier to collect (see [1] for timings about point supervision) and hence more versatile, and are better to upscale the training set. On the other hand, weak annotations are not necessarily reliable nor useful, because the annotation process is not exhaustive and decisions are made by the annotator.

Therefore, training a semantic segmentation pipeline in a weak supervision setting requires specific training strategies. Different strategies exist in the literature: adapting the DCNN architecture for the weakly supervised setting [10], changing the loss function of an existing DCNN architec-

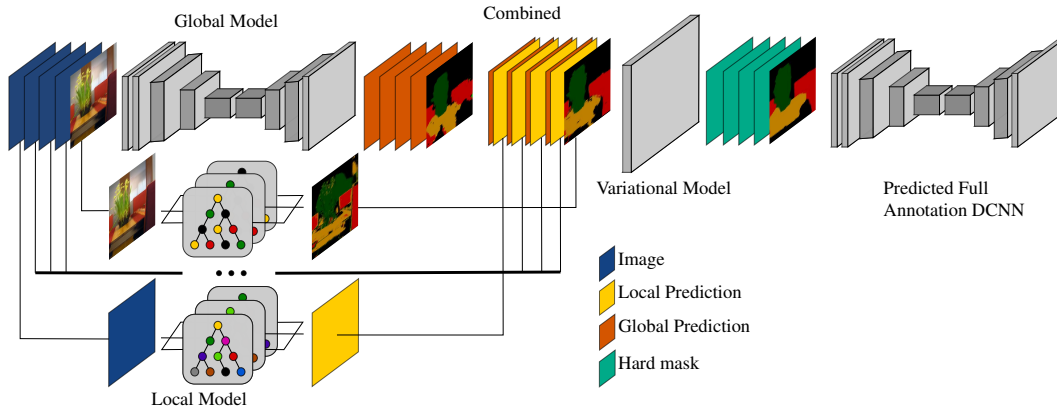


Figure 1. Predictive Annotator Models. Global and local models are trained on weak annotations. The predicted full annotations are subsequently used to train a DCNN for semantic segmentation.

ture to compensate for the information not contained in the weak annotations (*e.g.* [1] use objectness for point supervision and other higher-level priors, [29] designed a new loss function inspired by "shallow" segmentation), or post-processing the weak annotations to generate full ones to train an existing DCNN (*e.g.* bounding box annotations propagated by GrabCut [21] or other strategies [12], scribble annotations propagated by super-pixels and a variational model [16]).

1.2. (Semi-)interactive Segmentation

(Semi-)interactive segmentation can be seen as a boundary case of the weakly-supervised setting: the goal is to segment an image from the annotations (points, bounding box, scribbles, *etc.*) provided online by a human. This problem has triggered methods that can propagate the input annotations at interactive rate, and benefit from iterating the process on the same image by refining the segmentation after each user's input [27]. However, most interactive segmentation frameworks are designed for foreground extraction, *i.e.* for a two-class segmentation problem [27, 24]. Multi-class interactive segmentation frameworks are more recent and perform well at interactive rate [20].

State-of-the-art interactive segmentation frameworks are in essence *Bayesian* and *variational*. In the interactive setting, the amount of training data is low (reduced to the user inputs, such as bounding boxes [24], scribbles [30, 27], *etc.*) and makes the prediction for the unlabelled pixels uncertain. Therefore, Bayesian models are an attractive paradigm for this task, as they allow incorporating prior knowledge (*e.g.* boundary length [20], spatial semantic relation [5] and co-occurrence [15], appearance and smoothness in color space [13]) that facilitates the predictions when the semantic model alone is uncertain. In the interactive setting, the amount of computation time is also limited. Therefore, maximum *a posteriori* (MAP) is the inferential paradigm of choice because it allows leveraging efficient algorithms

operating at interactive rates [20]. Solving the associated MAP problem amounts to finding the semantic segmentation achieving an optimal trade-off between goodness-of-fit and consistency with the prior knowledge.

1.3. Goals and Contributions

In this work we tackle the problem of training a DCNN for the semantic segmentation problem in a weakly supervised setting, see [9] for a recent review and the references therein. Our main focus is on scribble annotations for which annotation data are available for the PASCAL VOC data set. Among the possible strategies described in Sec. 1.1, we follow the strategy consisting in post-processing the weak annotations to generate full annotations to train a subsequent DCNN from scribbles.

Our goal is not to emphasise a particular architecture, or algorithm that can achieve or beat the state-of-the-art, but rather to *identify simple ingredients necessary to close the gap between the baseline accuracy achievable by training the network on the weak annotations only (lower bound) and the accuracy obtained by training on the fully annotated training set (upper bound)*. Our motivation is that by simply using a newer version of DeepLab, *i.e.* DeepLabV2 [4], we obtain a baseline accuracy (64.3%, see Tab. 1) that is already higher than the original Scribble-Sup paper [16] (63.1%) and comparable to the most recent state-of-the-art [29] (65.1%), both using DeepLabV1, *i.e.* DeepLab-MSc-CRF-LargeFOV [4, 16, 29]. The main difference between the two architectures is that DeepLabV2 adapts ResNet-101 [8] instead of VGG-16 [28] and combines *atrous* convolution at multiple scales using Atrous Spatial Pyramid Pooling (ASPP).

In this work, we present a set of well-grounded experiments aiming at deciphering the ingredients necessary to close the aforementioned accuracy gap. We obtain state-of-the-art results recently established for scribble weak annotations by [29]: we obtain a gap in mIoU of 2.4% without

CRF (2.8% in [29]), and 2.9% with CRF post-processing (2.3% in [29]), see Tab. 2. However, we obtained such results by following a completely different path from [29]: *regularisation* of the predictive models used to generate the full annotations using Bayesian variational models; *combining* local (*i.e.* trained on an image-level) and global (*i.e.* trained on the data set level) predictive models to generate the full annotations.

2. Methods

2.1. Weakly-Supervised Scenario: Terminology and Measures.

In this work, we tackle the weakly-supervised semantic segmentation problem by following the strategy consisting in generating a fully annotated training set from weak annotations to train a subsequent DCNN.

Terminology. To disentangle the different levels of training, we captured the essence of the weak supervision process by introducing new terms: Weak Annotations (WAs) are used to generate Predicted Full Annotations (PFAs) that are otherwise provided by a human in a fully supervised scenario (Human Full Annotations (HFAs)). PFAs are made by a Predictive Annotator Model (PAM) that is either *local* (trained on each image) or *global* (trained on the whole training set). Fig. 1 shows a PAM combining all the specific building blocks within the same pipeline.

Defining the Gap between the fully- and weakly-supervised scenario. We aim at unravelling the ingredients required to train a DCNN on WAs that achieves performances comparable to *the same* DCNN trained on HFAs. After training, we call the resulting networks Weak Annotation DCNN (WA-DCNN) and Human Full Annotation DCNN (HFA-DCNN) respectively. The WA-DCNN defines a lower bound in quality, *i.e.* the baseline obtained solely on the WAs. The HFA-DCNN defines an upper bound in quality, because it is trained on the fully annotated training set. The difference between these two models defines a *gap in quality* that we attempt to close by using PAMs. The networks trained on the resulting PFAs are called Predicted Full Annotation DCNNs (PFA-DCNNs).

Measuring the Quality of PAMs. In addition to the classical evaluation on the validation set, it is important to evaluate the quality on the training set, *before* and *after* training on the WAs, because this provides a measure of the capability of the network to learn from the data predicted by the PAMs.

2.2. Data and Weak Annotations

We use the PASCAL VOC data set [6] because scribble WAs are publicly available from [16].

Curated WAs: Assessing Human Annotation Errors.

Weak annotations typically contain errors. For scribbles, two sources of errors are possible: assigning the wrong class or annotating multiple classes with one stroke. To assess the impact of human annotation errors on the segmentation performances, we assemble a curated training set: we use the scribbling positions but retrieve their class label from the ground truth. Furthermore, we require that at least all classes available in the ground truth are labelled, otherwise we drop the image from the training set. As a result, the curated training set contains 10489 instead of 10582 images.

We always report results about the best strategy for both the curated and the original scribbles (Tab. 1, lines 8/9 and 12/13, Tab. 2). However, for the sake of simplicity we show the results about the different experiments that lead us to identifying our best strategy only on the curated dataset (Tab. 1, lines 3–9).

2.3. Predictive Annotator Models: Random Forest (RF) and DeepLab

2.3.1 Local PAMs: Random Forest.

In interactive image segmentation two PAMs are common: Gaussian Mixture Models (GMMs) [24, 19] and RF classifiers [3, 26]. We use RF instead of GMM because RF trains quickly even with high dimensional data and provides a feature importance score enabling feature ranking. We use the custom *Gini feature importance score* available in python in `scikit-learn`. The features found in DCNNs trained for classification display desirable properties such as compositionality, invariance and class discrimination for ascending layers [33]. The first-layer features contain low-level image filters for different colour patterns *e.g.* edge or corner filters. Thus, we propose using the first-layer features of VGG-16 [28] and AlexNet [14] to train the RF classifier on each image. We use a forest consisting of 50 trees and apply the feature importance score to train the model on the 100 most informative one out of 160. Santner *et al.* [26, 27] use 30, 100 and 250 trees. We have observed that using 50 trees and 100 features leads to finer-grained predictions and decreases the amount of strong false positives and false negatives, *i.e.* class predictions with probability estimates of 0.0 or 1.0, preventing further improvement by the variation models.

2.3.2 Global PAMs: DeepLab.

A state-of-the-art DCNN in supervised semantic segmentation is DeepLab [4]. Different versions of DeepLab are used in weakly-, semi-, or fully-supervised settings [16, 21]. We propose to use a simplified version of DeepLabV2 as the global PAM. The architecture is based on ResNet-101 connected with an ASPP module with four branches (*atrous* rates $r \in \{6, 12, 18, 24\}$) and a bilinear upsampling to match the input resolution. We disable multi-scaling and post-processing using Fully Connected Conditional Random Field (FC-CRF) [13]. DeepLab requires a full annotation for training. In order to train DeepLab solely on WAs we use the scribbles at the labelled pixels and assign the `ignore` class to the unlabelled pixels otherwise. We initialise the model using the parameters of ResNet-101 pre-trained on ImageNet [25]. We use random initialisation for all other parameters. In particular, we avoid pre-training DeepLabV2 on any segmentation dataset such as MS-COCO [4]. We modify a publicly available TensorFlow implementation of DeepLabV2 [32]. Our training looks as follows: 20k training iterations, a batch size of 10, momentum of 0.9, weight decay of 5×10^{-4} and a *poly* learning rate policy with power 0.9, see [4]. We tuned the learning rate and the other parameters *only for the baseline trained on scribbles* and we kept the same parameters for all the models shown in Tab. 1. We always report the performance *after a fixed number of training iterations* (20k). We tested learning rates between 2.5×10^{-4} and 7.5×10^{-4} . We obtained the best performances on the validation set for a learning rate of 6.25×10^{-4} . We also enable data augmentation by randomly mirroring and scaling the input data. We calculate the loss after bilinear upsampling, (input resolution 321×321).

2.4. Regularisation of the PAMs.

A Bayesian model for semantic segmentation consists of a *semantic model* encoding how well pixels fit in their assigned classes (encoded in a *data-fitting term*) and a consistency model encoding how well a particular segmentation fits some desired prior knowledge (encoded in a *regularisation term*). User inputs are used to train the semantic model derived from the predictive models, described in Sec. 2.3, that learn how pixels should be grouped together. The regularisation helps when the semantic model is uncertain about how to assign a class to a pixel, in particular when the amount of data to calibrate the semantic model is low, as for the local models. In this work we compare two popular variational models for the regularisation of the predictive models: the Potts [20] and the FC-CRF [13] models. Both share the same data-fitting term, but differ in regularisation.

Bayesian Data-Fitting Terms. The data-fitting term for semantic segmentation writes as the sum over the set of pixels, denoted \mathcal{I} , of the scalar product between the semantic *segmentation mask* vector, denoted M_i , and the negative *log-labelling probability* vector, denoted P_i , see for example [20]:

$$\mathcal{E}_d(\mathbf{M}) := \sum_{i \in \mathcal{I}} \langle -\log P_i, M_i \rangle. \quad (1)$$

The vector M_i represents a valid semantic segmentation hypothesis, *i.e.* an element of the unit probability simplex. When at each pixel the mask vector contains a single one and zeros otherwise, the segmentation is called *hard*, and *soft* otherwise. The vector P_i encodes the semantic segmentation model, *i.e.* P_{ic} is the probability of assigning class c at pixel i .

Potts regularisation. The Potts model penalises the total length of the interface between the classes and is popular for its simplicity and the various efficient algorithms to compute the associated MAP (see [20]). This regularisation amounts to summing the weighted total variation of the mask for each class:

$$\mathcal{E}_r^{\text{TV}}(\mathbf{M}) := \lambda \sum_{c \in \mathcal{C}} \text{TV}_g(M_c), \quad (2)$$

where g is the edge-stop function defined as $g_i = \exp(-\eta|\nabla \mathbf{I}|_i)$.

FC-CRF regularisation. For comparison, we also use the more complex regularisation of the FC-CRF model [13], popular in the literature as a post-processing that recovers detailed features from the blobby predictions of a DCNN. This regulariser is defined as

$$\mathcal{E}_r^{\text{FC-CRF}}(\mathbf{M}) := \sum_{c \in \mathcal{C}} \sum_{(i,j) \in \mathcal{I}^2} [M_i \neq M_j] (w_1 \mathbf{A}_{ij} + w_2 \mathbf{S}_{ij}), \quad (3)$$

where $\mathbf{A}_{ij} := \exp(-d_{ij}^2/2\sigma_\alpha^2 - \delta_{ij}^2/2\sigma_\beta^2)$ and $\mathbf{S}_{ij} := \exp(-d_{ij}^2/2\sigma_\gamma^2)$ are defined as the *appearance* and *smoothness* kernels respectively, with d_{ij} is the Euclidean distance between the locations of pixel i and j , and δ_{ij} is the Euclidean distance in color space between pixel i and j . This prior tends to group together nearby pixels with similar colours (appearance kernel), while penalising small clusters (smoothness kernel).

MAP predictions. For both models we solve the associated MAP problem by solving an optimisation problem aiming at finding the optimal trade-off between fitting the data, driven by \mathcal{E}_d see Eq. (1), and regularisation, driven either by Eq. (2) (Potts model) or Eq. (3) (FC-CRF model).

	Training Data	PAM		Regularisation		ID	PFA	DCNN		Gap	
		Local	Global	Potts	FC-CRF			Train	Train	Validation	↓
Curated	HFA					1	100	80.7	71.5	4.4	—
	WA					2	100	74.8	67.1	—	4.4
		✓				3	61.5	67.8	61.0	-6.1	10.5
		✓		✓		4	73.3	70.9	63.3	-3.8	8.2
			✓	✓		5	79.4	74.6	67.8	0.7	3.7
	PFA		✓		✓	6	79.6	75.6	68.2	1.1	3.3
		✓	✓			7	81.0	76.4	69.2	2.1	2.3
		✓	✓	✓		8	84.2	76.8	69.7	2.6	1.8
		✓	✓		✓	9	83.9	77.6	70.0	2.9	1.5
Original	HFA					10	100	80.7	71.5	7.2	—
	WA					11	95.4	71.7	64.3	—	7.2
		✓	✓	✓		12	81.6	76.4	68.8	4.5	2.7
	PFA	✓	✓		✓	13	81.4	76.5	69.1	4.8	2.4

Table 1. Towards Closing the Gap. We report the mIoU [%]. The gap is shown in light grey, for both the curated and the original WA [16]. The ↓ shows the difference with the *baseline*. The ↑ shows the difference to the upper bound. We report the best mIoU among different regularisation parameters for the Potts model (see 2.4). The column PFA reports the mIoU of the PFAs of the training images produced by the PAMs. The column ID helps reference rows in the main text. See Fig. 2 for class-specific results.

We solve the Potts MAP problem using the strategy described in [23]. The regularisation parameter λ is selected by a grid search on all images in the training set. We use the parameters that achieve the highest mIoU on the PFAs: $\lambda = 10$ when the predictive model contains local predictions and $\lambda = 50$ when only the global model is used. We use for the edge stop function the parameter $\eta = 0.01$. For the FC-CRF MAP problem, we use the implementation of [13] found at [2]. We selected the parameters of the FC-CRF by grid search on a subset of the PFAs obtained from the combined model and use the same parameters for all experiments. The parameters are: $w_1 = 3$, $\sigma_\alpha = 30$, $\sigma_\beta = 5$, $w_2 = 5$ and $\sigma_\gamma = 2$.

Training from the PAMs. We use the trained PAMs described in Sec. 2.3 to parametrise the variational models defined in Sec. 2.4: their soft predictions are used to compute the labelling cost defined in Eq. (1) by computing the negative log-probability.

2.5. Training DeepLab on FA

In this work we use the same DCNN for the global PAM (called WA-DCNN) and the model used in production (called PFA-DCNN). The reason is that we want to study how to close the gap. The only difference is that PFA-DCNN is trained on full annotations generated by different PAMs, whereas WA-DCNN is trained solely on weak annotations (see Fig. 1 and Tab. 1).

3. Results

As discussed in Sec. 2, HFA-DCNN corresponds to DeepLabV2 trained on the HFA (see Sec. 2.3.2). We obtain a mIoU of 71.5% on the validation set (see Tab. 1, lines 1 and 10), establishing an upper bound in segmentation accuracy. However, investigating strategies to train a DCNN on WA (*i.e.* WA-DCNN) to achieve performances comparable to a DCNN trained on fully annotated training set (*i.e.* HFA-DCNN) requires establishing a *baseline*.

3.1. Establishing the Baseline: WA-DCNN

On the original scribbles [16], the WA-DCNN achieves a mIoU of 64.3% on the validation set, establishing a gap of 7.2% (see Tab. 1, line 11). On the curated WAs the baseline increases to 67.1% and reduces the gap to 4.4% (see Tab. 1, line 2). As expected, the gap is 2.8% smaller for the curated data set. This gives a first *insight on the impact of the errors in the WA on the resulting trained model*. In order to factor out this effect, we perform the systematic experimental study combining different ingredients on the curated training set. However, because such training sets do not exist in practice, we always report the results for our best strategies on the original training set provided by [16], see Tab. 1 (lines 12 and 13), and Tab. 2. Having established the baseline, we need to assess the quality of the full annotations of the training set generated by the PAMs. The baseline model (WA-DCNN, Tab. 1, line 2) can be used to annotate the unlabelled pixels in the training set, where we can measure the mIoU of these PFAs, and obtain 74.8% (see Tab. 1, line 2).



Figure 2. Intersection over Union (IoU) evaluated on the training set. *Before* training, we report the IoU of the predicted full annotations (PFAs) for the local, global and combined annotator models, with or without TV regularisation (Potts model). *After* training, we report the IoU of the DCNN trained on each PFA. The classes are ordered according to the IoU obtained by the best strategy (RF-CNN-TV) in decreasing order from Background (abbreviated Bg) to Chair. The left panel on the middle row shows the IoU of the baseline. The mean IoU (mIoU) are shown with vertical lines. The gap (see table 1 in the paper) is shown as a grey rectangle.

3.2. DCNNs Trained on Local PFAs

We report the mIoU of the PFAs on the training images to assess the impact of their quality on the performance of DeeplabV2 (column PFA in Tab. 1). On average, RF generates PFAs with a mIoU of 61.5% (see Tab. 1, line 3) without regularisation, and a mIoU of 73.3% with a Potts regu-

lariser (*i.e.* best Potts model with $\lambda = 10$, see Tab. 1, line 4). Therefore, regularisation boosts the RF predictions by 11.8% on average. However, after training DeepLab on the local PFAs without regularisation leads to a mIoU of 61.0% on the validation set, a score below the baseline by 6.1% (see Tab. 1, line 3). Regularisation boosts the mIoU by 2.3% up to 63.3%, but still lags behind the baseline by 3.8% (see

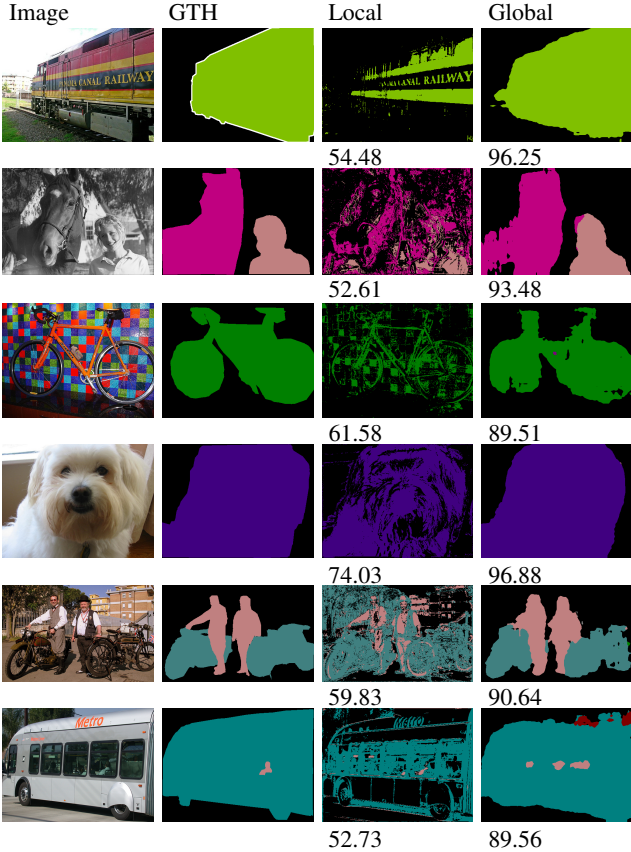


Figure 3. Examples where global PFAs have a higher pixel accuracy than the local ones.

Tab. 1, line 4).

These results suggest that the PFAs are not sufficient to train a PFA-DCNN better than the baseline, despite the additional annotations generated by the local PAM. This probably comes from the annotation errors introduced by the local PAM. In Fig. 3 we show examples of images where the local PAM is worse than the baseline. To quantify this effect we compare the pixel accuracy of the PFAs generated by the local and global PAMs. In Fig. 4 (left panel), we observe for most images that the pixel accuracy is best for the baseline (*i.e.* the global PAM).

Fig. 5 illustrates the effect of poor WAs. We visualise the WAs both in image space and feature space (embedded in 2D with t-Distributed Neighbor Embedding (T-SNE) [18]). It shows that the scribbles sample only poorly the feature space. Sampling the missed regions and visualising the annotations in the original image shows that the WAs miss important semantic information.

Poor scribbling is probably the reason why a PFA-DCNN trained on local PFAs lags behind the *baseline*. Nonetheless, regularisation has a beneficial effect and added a boosting of 2.3%. Therefore, we investigate next the ef-

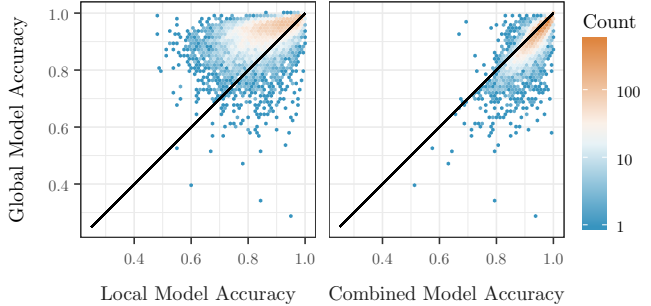


Figure 4. Comparison of the pixel accuracy computed for each image in the PASCAL VOC training set, between the global PAM (WA-DCNN) and the local PAM (RF) or combined PAM (RF+WA-DCNN). The diagonal shows the equal accuracy cutoff.

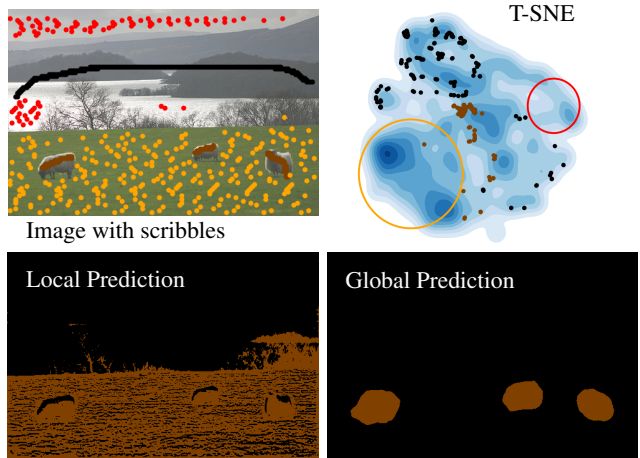


Figure 5. Case where the global PFA trained on scribbles (brown: sheep, black: background) is better than the local one. The scribbles are shown in image space and in feature space (embedded with T-SNE). The circles (orange and red) show regions not covered by the WA. Pixel in these regions are shown as red and orange dots.

fect of regularisation on the global PAM (*i.e.* WA-DCNN).

3.3. Regularising Global PAMs improves only Marginally

Regularising WA-DCNN boosts the PFAs mIoU by 4.6% up to 79.4% (see Tab. 1, line 5). Training DeepLab on these PFAs results in a mIoU exceeding the baseline, but only marginally by 0.7%, up to 67.8%. To test if a more complex regulariser leads to a larger improvement, we repeat the experiments using the FC-CRF instead of the Potts model. The quality of PFAs and of the subsequently trained DCNN is marginally higher, 79.6% and 68.2% respectively (see Tab. 1, line 6). Therefore, using a global PAMs is superior to a local one, and regularisation enhances the quality of the PFA, leading to a better PFA-DCNN. However, the improvement compared to the *baseline* is small and the gaps



Figure 6. Examples where the combined PFAs have a higher pixel accuracy than either the local or global ones.

are still 3.7% (Potts) and 3.3% (FC-CRF).

We observed in Fig. 4 that the pixel accuracy of the PFAs generated by the global PAM is in general higher (above the diagonal) than the local PFAs. However, there are images where the local PAMs achieve better annotations (below the diagonal). This suggests that the local and global PAMs are complementary. To test this idea we show the pixel accuracy of the PFAs obtained by averaging their predictions. Fig. 4 shows that combining local and global predictions improves compared to the global PAM only. Fig. 6 shows images where the local and global PAMs achieve a comparable score, but the combined predictions are superior.

3.4. Combining Local and Global PAMs improves PFAs

Without regularisation, combining PFAs achieves a mIoU of 81% (RF: 61% and WA-DCNN: 74.8%) and the subsequently trained PFA-DCNN achieves 69.2% on the validation set (see Tab. 1, line 7). Hence, combining local and global PAMs boosts the quality of the PFAs substantially. The model trained on these improved PFAs outperforms the baseline by 2.1%. Regularisation increases the PFA quality with the Potts model to 84.2% and with the FC-CRF to 83.9%, leading to trained models with a mIoU

of 69.7% and 70.0% on the validation set (see Tab. 1, lines 8 and 9). As a control, we repeat the experiments with the non-curated WAs and report trained models with a mIoU on the validation set of 68.8% (Potts) and 69.1% (FC-CRF), see Tab. 1 (lines 12 and 13).

Hence, combining local and global PAMs has a larger impact than regularisation alone. However, in synergy, these two ingredients lead to trained models that reduce the gap to 1.8% and 1.5% and improve the *baseline* by 2.6% (Potts) and 2.9% (FC-CRF). The improvement with respect to the baseline is even higher for the non-curated WAs (see Tab. 1 lines 12 and 13). We show in Fig. 2 class-specific results.

3.5. Closing the Gap by increasing the Amount of Weak Annotations

Closing the gap has been reported only recently at CVPR17 for bounding boxes [12]. To close the gap, [12] requires 10× more training images than their baseline. On PASCAL VOC12, publicly available scribble annotations are provided only in [16]. Decreasing the amount of scribbles is achieved in [16] by shortening the strokes, but increasing the number of pixels annotated by scribbles is not available. Instead, to vary the amount of WA we randomly sample the full annotation for each image, by respecting the proportions between classes and ensuring that there is at least one pixel per class annotated. This strategy imitates the pixel statistics of the scribbles generated in [16], but destroys at an image-level the spatial correlation of the annotated pixels.

In Fig. 7 we observe that each model outperforms the baseline (oscillating around 67.5%), even for fewer annotations. The model trained on the randomly sampled point WAs with an annotation effort of 3.1% already achieves 71.4% mIoU on the validation set and decreases the gap to only 0.1%. Although this way of generating additional WAs is not possible in practice, this experiments shows that the baseline model seems insensitive to varying amounts of annotated pixels in this range of annotation effort, whereas the strategy combining local and global PAMs with regularisation can quickly benefit from these additional annotations, the best performing model being the simple Potts model.

4. Conclusions and Discussion

We tackle a recent and important problem in semantic segmentation: *Training a DCNN designed for full annotations from weak annotations and yet get comparable performances.* To disentangle the different levels of training, we captured the essence of the weak supervision process by introducing new terms, see Sec. 2.1.

Our comprehensive experimental design (Tab. 1) accounts for the individual contributions of each component

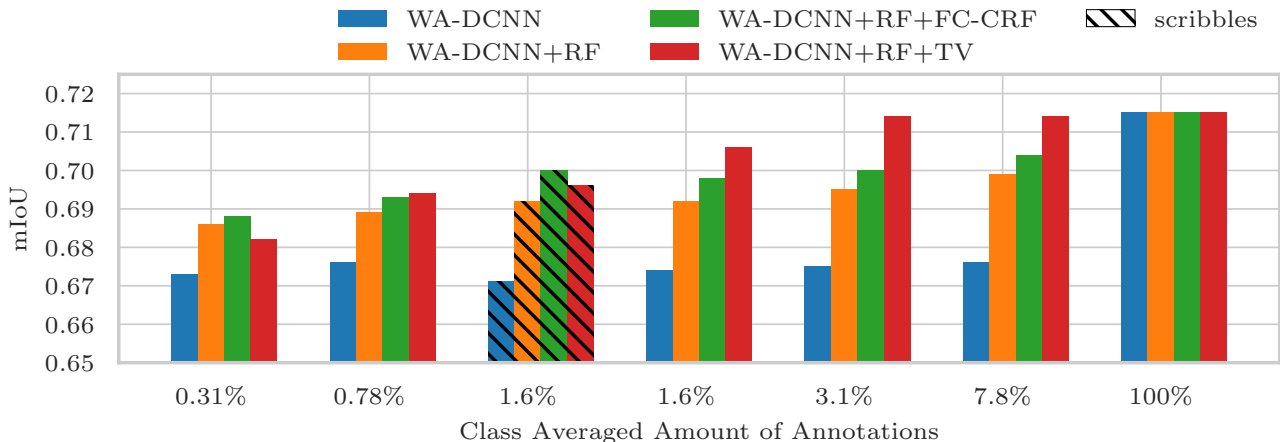


Figure 7. DCNNs trained on PFAs produced with varying amount of weak labels.

Model	FC-CRF	WAs	FA Validation	WA Validation (Gap)	FA Test	WA Test (Gap)
ScribbleSup [16]	✓	Scribbles	68.7	63.1 (5.6)	—	—
SimpleDoesIt [12]	✓	BBoxes	69.1	65.7 (3.4)	70.5	67.5 (3.0)
NCL [29]	—	Scribbles	75.6	72.8 (2.8)	—	—
NCL [29]	✓	Scribbles	76.8	74.5 (2.3)	—	—
Ours (Original)	—	Scribbles	71.5	69.1 (2.4)	73.1	70.4 (2.7)
Ours (Original)	✓	Scribbles	73.4	70.5 (2.9)	75.0	72.5 (2.5)
Ours (Curated)	—	Scribbles	71.5	70.0 (1.5)	—	—

Table 2. Comparison to the state-of-the-art methods in weakly supervised semantic segmentation. We report the mIoU [%] on the validation and test set of PASCAL VOC12 when available. FA Val. means the accuracy of the DCNN trained on the fully-annotated training set and evaluated on the validation set, and WA Val. is the accuracy of the same network trained on weak annotations and evaluated on the validation set. The gap between the two is shown in parenthesis.

and quantifies the impact of human annotation errors (original vs. curated WAs). We show that human annotation errors degrade the performance of the baseline by 2.8 but our best performance is decreased only by 0.9 (see Tab. 1), showing the robustness of our approach. This design also allowed us to identify an unexpected interaction between the local and the global PAMs that conspire to boost the overall accuracy (Tab. 1, Fig. 3, 4, 5 and 6).

To compare our results with the recent literature, we also report the results with Conditional Random Field (CRF) post-processing on the validation and test sets, see Tab. 2. In terms of gaps, we obtained state-of-the-art results comparable to the ones obtained recently by [29] on scribbles. The difference in absolute mIoU is probably due to the fact that [29] uses multi-scaling in DeepLab, and we do not. However, we obtained comparable performances following a different path: in [29] they designed new loss functions adapted to the weakly-supervised semantic segmentation, whereas we unravelled a general principle, combining local and global PAMs, that could potentially be applied to other

settings. Therefore, we could expect that combining both strategies could benefit from one another.

Closing this gap has been reported only recently at CVPR17 for bounding boxes [12], by requiring 10× more training images. However, scribbles allow increasing the amount of WAs without increasing the number of training images. We explored such a possibility by simulating varying amounts of labelled pixels that respect human annotators class frequency statistics (Fig. 7). To close the gap, we require only 2–5× more annotated pixels on the same training set, as opposed to [12]. However, closing the gap in practice remains an open problem.

References

- [1] A. Bearman, O. Russakovsky, V. Ferrari, and L. Fei-Fei. What’s the Point: Semantic Segmentation with Point Supervision. In *Computer Vision – ECCV 2016*, pages 549–565, 2016.
- [2] L. Beyer. PyDenseCRF. <https://github.com/lucasb-eyer/pydensecrf>, 2018.

- [3] L. Breiman. Random forests. *Machine Learning*, 45(1):5–32, Oct 2001.
- [4] L.-C. Chen, G. Papandreou, I. Kokkinos, K. Murphy, and A. L. Yuille. DeepLab: Semantic Image Segmentation with Deep Convolutional Nets, Atrous Convolution, and Fully Connected CRFs. *IEEE Transactions on Pattern Analysis and Machine Intelligence*, 40(4):834–848, April 2018.
- [5] J. Diebold, C. Nieuwenhuis, and D. Cremers. Midrange Geometric Interactions for Semantic Segmentation: Constraints for Continuous Multi-label Optimization. *International Journal of Computer Vision*, 117(3):199–225, 2016.
- [6] M. Everingham, L. Van Gool, C. K. I. Williams, J. Winn, and A. Zisserman. The Pascal Visual Object Classes (VOC) Challenge. *International Journal of Computer Vision*, 88(2):303–338, Jun 2010.
- [7] A. Garcia-Garcia, S. Orts-Escolano, S. Oprea, V. Villena-Martinez, and J. Garcia-Rodriguez. A Review on Deep Learning Techniques Applied to Semantic Segmentation. *arXiv preprint*, pages 1–23, 2017.
- [8] K. He, X. Zhang, S. Ren, and J. Sun. Deep Residual Learning for Image Recognition. In *The IEEE Conference on Computer Vision and Pattern Recognition (CVPR)*, 2016.
- [9] S. Hong, S. Kwak, and B. Han. Weakly Supervised Learning with Deep Convolutional Neural Networks for Semantic Segmentation: Understanding Semantic Layout of Images with Minimum Human Supervision. *IEEE Signal Processing Magazine*, 34:39–49, nov 2017.
- [10] S. Hong, H. Noh, and B. Han. Decoupled Deep Neural Network for Semi-supervised Semantic Segmentation. In *Proceedings of the 28th International Conference on Neural Information Processing Systems - Volume 1, NIPS’15*, pages 1495–1503, Cambridge, MA, USA, 2015. MIT Press.
- [11] Z. Huang, X. Wang, J. Wang, W. Liu, and J. Wang. Weakly-Supervised Semantic Segmentation Network With Deep Seeded Region Growing. In *The IEEE Conference on Computer Vision and Pattern Recognition (CVPR)*, June 2018.
- [12] A. Khoreva, R. Benenson, J. Hosang, M. Hein, and B. Schiele. Simple Does It: Weakly Supervised Instance and Semantic Segmentation. In *The IEEE Conference on Computer Vision and Pattern Recognition (CVPR)*, July 2017.
- [13] P. Krähenbühl and V. Koltun. Efficient inference in fully connected CRFs with Gaussian edge potentials. In J. Shawe-Taylor, R. S. Zemel, P. L. Bartlett, F. Pereira, and K. Q. Weinberger, editors, *Advances in Neural Information Processing Systems 24*, pages 109–117. Curran Associates, Inc., 2011.
- [14] A. Krizhevsky, I. Sutskever, and G. E. Hinton. ImageNet Classification with Deep Convolutional Neural Networks. In F. Pereira, C. J. C. Burges, L. Bottou, and K. Q. Weinberger, editors, *Advances in Neural Information Processing Systems 25*, pages 1097–1105. Curran Associates, Inc., 2012.
- [15] L. Ladicky, C. Russell, P. Kohli, and P. H. S. Torr. Graph cut based inference with co-occurrence statistics. In K. Daniilidis, P. Maragos, and N. Paragios, editors, *Computer Vision – ECCV 2010*, pages 239–253, Berlin, Heidelberg, 2010. Springer Berlin Heidelberg.
- [16] D. Lin, J. Dai, J. Jia, K. He, and J. Sun. ScribbleSup: Scribble-Supervised Convolutional Networks for Semantic Segmentation. In *The IEEE Conference on Computer Vision and Pattern Recognition (CVPR)*, June 2016.
- [17] T.-Y. Lin, M. Maire, S. Belongie, J. Hays, P. Perona, D. Ramanan, P. Dollár, and C. L. Zitnick. Microsoft COCO: Common Objects in Context. In D. Fleet, T. Pajdla, B. Schiele, and T. Tuytelaars, editors, *Computer Vision – ECCV 2014*, pages 740–755. Springer International Publishing, 2014.
- [18] L. V. D. Maaten and G. Hinton. Visualizing Data using t-SNE. *Journal of machine learning research*, 620(1):2579–2605, 2008.
- [19] C. Nieuwenhuis and D. Cremers. Spatially varying color distributions for interactive multilabel segmentation. *IEEE Transactions on Pattern Analysis and Machine Intelligence*, 35(5):1234–1247, 2013.
- [20] C. Nieuwenhuis, E. Töppe, and D. Cremers. A survey and comparison of discrete and continuous multi-label optimization approaches for the Potts model. *International Journal of Computer Vision*, 104(3):233–240, 2013.
- [21] G. Papandreou, L.-C. Chen, K. P. Murphy, and A. L. Yuille. Weakly- and semi-supervised learning of a deep convolutional network for semantic image segmentation. In *The IEEE International Conference on Computer Vision (ICCV)*, December 2015.
- [22] D. Pathak, E. Shelhamer, J. Long, and T. Darrell. Fully Convolutional Multi-Class Multiple Instance Learning. *ArXiv e-prints*, Dec. 2014.
- [23] G. Paul, J. Cardinale, and I. F. Sbalzarini. An alternating split Bregman algorithm for multi-region segmentation. In *2011 Conference Record of the Forty Fifth Asilomar Conference on Signals, Systems and Computers (ASILOMAR)*, pages 426–430, Nov 2011.
- [24] C. Rother, V. Kolmogorov, and A. Blake. ”GrabCut”: Interactive Foreground Extraction Using Iterated Graph Cuts. *ACM Trans. Graph.*, 23(3):309–314, Aug. 2004.
- [25] O. Russakovsky, J. Deng, H. Su, J. Krause, S. Satheesh, S. Ma, Z. Huang, A. Karpathy, A. Khosla, M. Bernstein, A. C. Berg, and L. Fei-Fei. ImageNet Large Scale Visual Recognition Challenge. *International Journal of Computer Vision*, 115(3):211–252, Dec 2015.
- [26] J. Santner, T. Pock, and H. Bischof. Interactive multi-label segmentation. In R. Kimmel, R. Klette, and A. Sugimoto, editors, *Computer Vision – ACCV 2010*, pages 397–410, Berlin, Heidelberg, 2011. Springer Berlin Heidelberg.
- [27] J. Santner, M. Unger, T. Pock, C. Leistner, A. Saffari, and H. Bischof. Interactive texture segmentation using random forests and total variation. In *Proceedings of the British Machine Vision Conference*, pages 66.1–66.12. BMVA Press, 2009. doi:10.5244/C.23.66.
- [28] K. Simonyan and A. Zisserman. Very Deep Convolutional Networks for Large-Scale Image Recognition. In *International Conference on Learning Representations (ICRL)*, pages 1–14, 2015.
- [29] M. Tang, A. Djelouah, F. Perazzi, Y. Boykov, and C. Schroers. Normalized Cut Loss for Weakly-Supervised CNN Segmentation. In *The IEEE Conference on Computer Vision and Pattern Recognition (CVPR)*, June 2018.

- [30] M. Unger, T. Pock, W. Trobin, D. Cremers, and H. Bischof. TVSeg - Interactive Total Variation Based Image Segmentation. In *Proceedings of the British Machine Vision Conference*, pages 40.1–40.10. BMVA Press, 2008. doi:10.5244/C.22.40.
- [31] P. Vernaza and M. Chandraker. Learning Random-Walk Label Propagation for Weakly-Supervised Semantic Segmentation. In *The IEEE Conference on Computer Vision and Pattern Recognition (CVPR)*, July 2017.
- [32] Z. Wang. Deeplab-v2-ResNet-101-Tensorflow. <https://github.com/zhengyang-wang/Deeplab-v2--ResNet-101--Tensorflow>, 2018.
- [33] M. D. Zeiler and R. Fergus. Visualizing and understanding convolutional networks. In D. Fleet, T. Pajdla, B. Schiele, and T. Tuytelaars, editors, *Computer Vision – ECCV 2014*, pages 818–833, Cham, 2014. Springer International Publishing.

A. Appendix

A.0.1 DeepLab Predictions.

We show predictions of DeepLab trained from PFAs generated by the different strategies explored in the paper, see Fig. 8.

A.0.2 Comparing PFAs.

Fig. 9 shows the mIoU of the PFAs generated by the different strategies for the scribbles and the random point WAs. We show a similar trend as in Fig. 7 in the main paper showing the effect of the quality and quantity of the WAs on the segmentation quality, but evaluated for the PFAs (*i.e.* before training, evaluated on the training set). We observe that increasing the amount of annotations improves the RF predictions, whereas the WA-DCNN prediction quality remains the same. The Potts model is particularly effective for larger amounts of annotations compared to the FC-CRF.

In Fig. 2, we show a significant drop in Intersection over Union (IoU) only for a subset of classes (from **Bottle** to **Chair**). In Fig. 10 we compare the confusion matrices computed on the training set for the baseline (WA-DCNN), and the best strategy WA-DCNN+RF+Total Variation (TV), before and after training.

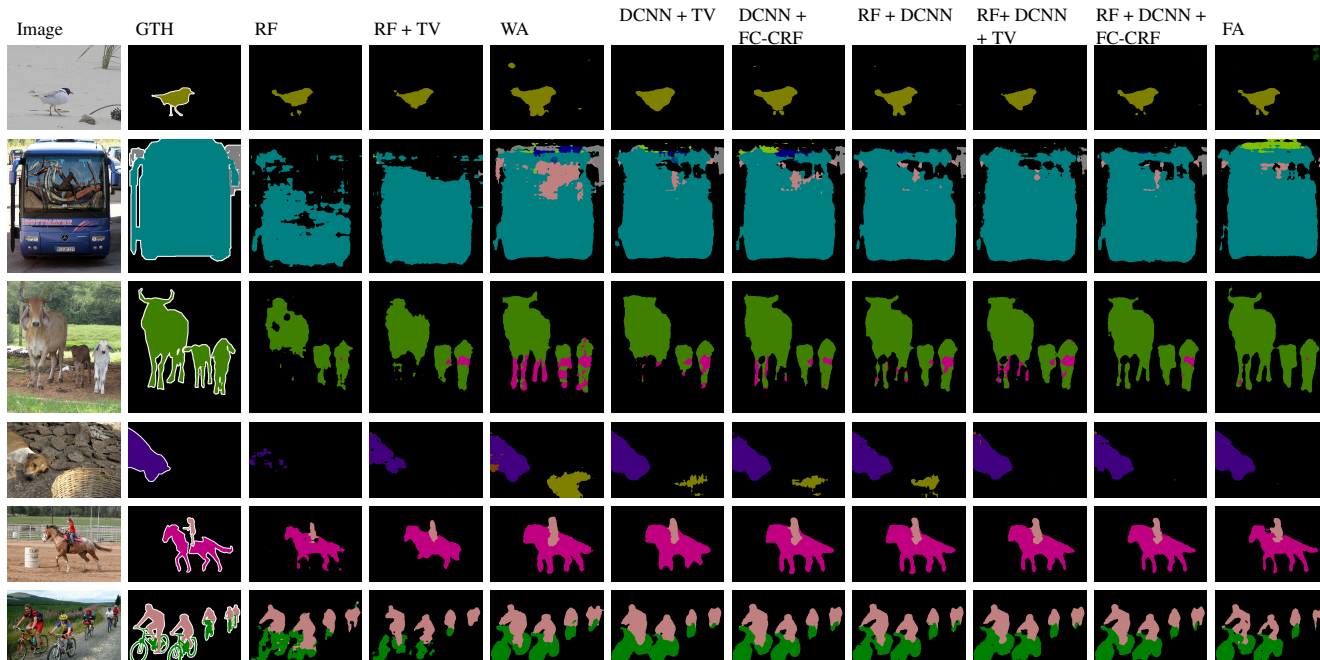


Figure 8. Sample predictions of the DCNN trained on the different Predictive Annotator Models. The images are part of the validation set.

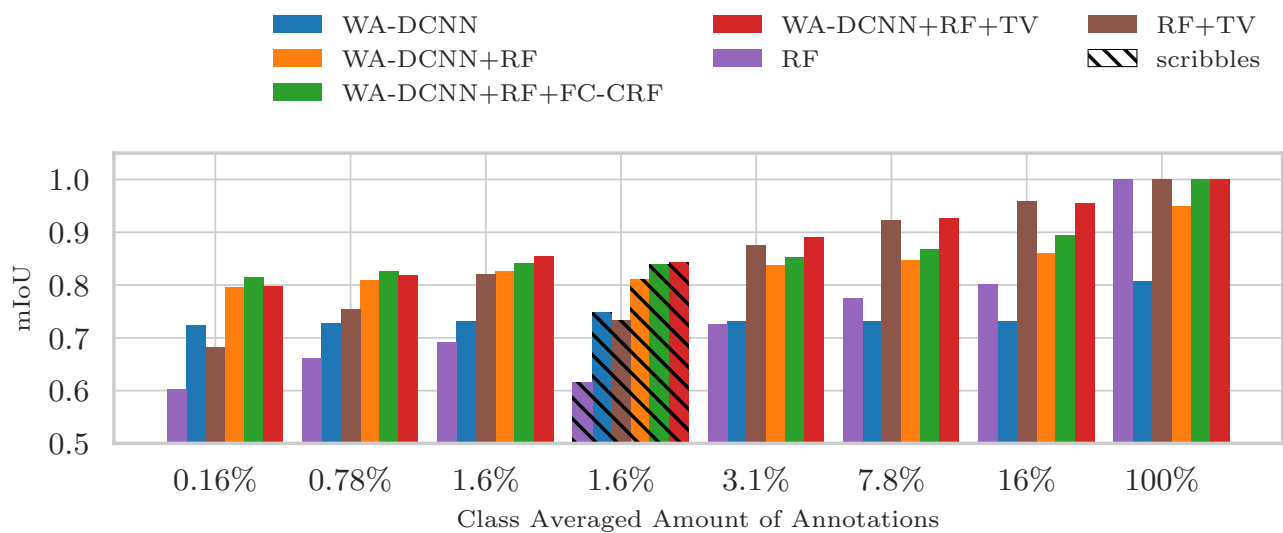


Figure 9. Quality of the Predicted Full Annotations generated by different PAMs and for varying amount of WAs.

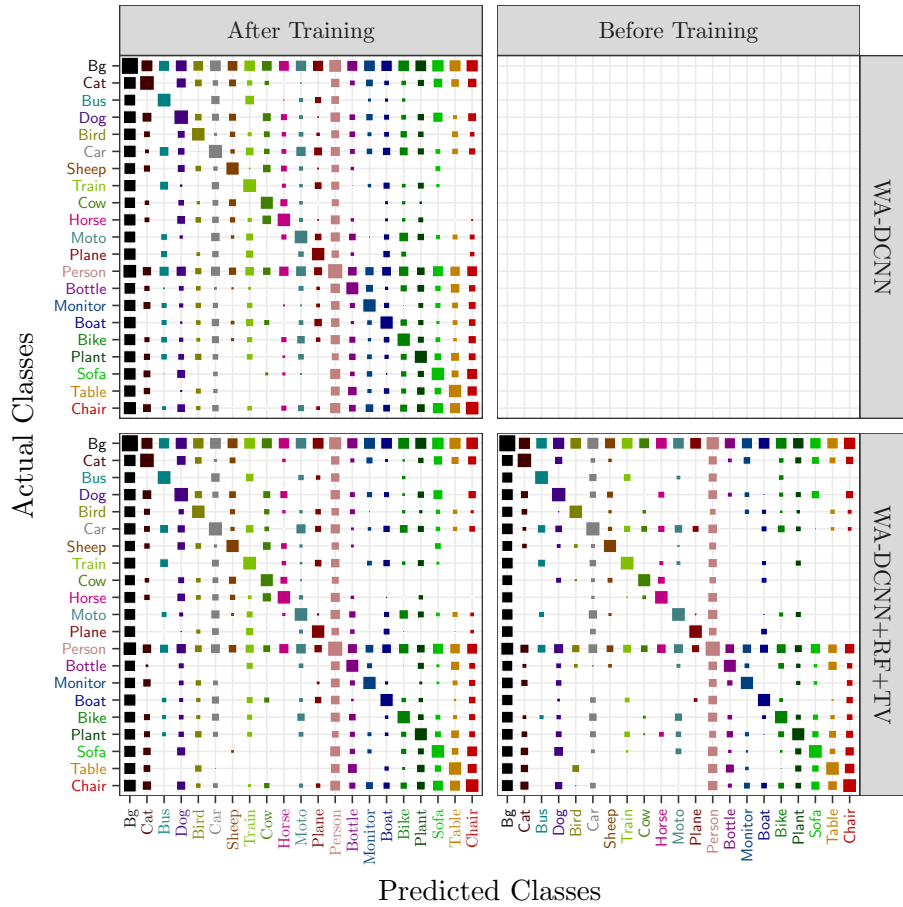


Figure 10. Comparison of the confusion matrices of WA-DCNN+RF+TV before and after training with the baseline WA-DCNN. The size of each square is proportional to the corresponding entry in the confusion matrix.